Research Square

Preprints are preliminary reports that have not undergone peer review.
They should not be considered conclusive, used to inform clinical practice,
or referenced by the media as validated information.

Adsorption of Digoxin by Activated carbon prepared from Walnut shell

Batoul Al-Tahan
Higher Institute for Applied Sciences and Technology
Ali Alkady
Higher Institute for Applied Sciences and Technology
Ibrahem Essa
Higher Institute for Applied Sciences and Technology
Hussein Khoder
Higher Institute for Applied Sciences and Technology
Akil Salloum
akil.salloum@hiast.edu.sy

Higher Institute for Applied Sciences and Technology

Research Article

Keywords: Activated carbon, Walnut shell, Digoxin, Adsorption, Phosphoric acid activation, Gastrointestinal decontamination

Posted Date: November 20th, 2026

DOI: https://doi.org/10.21203/rs.3.rs-11621006/v1

License: This work is licensed under a Creative Commons Attribution 4.0 International License.
Read Full License

Additional Declarations: No competing interests reported.

Adsorption of Digoxin by Activated carbon prepared from Walnut shell

Batoul Al-Tahan [a], Ali Alkady[b], Ibrahem Essa[c], Hussein Khoder[d], Akil Salloum[e]*

[a, b, c, d,e] *Higher Institute of Applied Sciences and Technology (HIAST), Damascus, Syria*

*Corresponding author: E-mail: akil.salloum@hiast.edu.sy

Abstract

To explore a low-cost candidate adsorbent for digoxin decontamination, this study evaluated the adsorption of digoxin from a simulated physiological buffer (PBS, pH 7.4) using activated carbon (AC) derived from walnut-shell biomass via food-grade phosphoric acid (H_3PO_4) activation. Optimization of preparation conditions yielded a material with a maximum iodine number of 895.65 mg/g at 400 °C and 35 wt% H_3PO_4, corresponding to an estimated specific surface area of ~1490 m²/g. An extensive washing protocol reduced residual acidity from the activating agent, resulting in a purified adsorbent with a near-neutral pH (7.0 ± 0.1). Under simulated physiological conditions (0.031 mg/mL digoxin, 25 °C), the synthesized AC demonstrated rapid, dose-dependent adsorption kinetics. At a dosage of 2 g, approximately 95% of digoxin was removed within 5 min, with residual concentrations approaching the analytical limit of detection (LOD). By 25–30 min, residual digoxin levels fell below the LOD, indicating a removal efficiency exceeding 95.5%. Under identical conditions, the commercial reference CARBOMIX showed 74–82% removal, compared with the prepared AC's apparent removal exceeding 95.5%. FTIR analysis confirmed the retention of oxygen-containing functional groups, while a point of zero charge (pHpzc) of 7.44 suggested a low net surface charge at physiological pH. Kinetic modeling revealed that adsorption data were best described by the non-linear pseudo-second-order model ($R^2 > 0.99$). With the exception of the CARBOMIX comparison, which was subsequently duplicated, all adsorption experiments were performed as single runs without replicates; therefore, the results should be regarded as exploratory and not statistically confirmed. These findings provide a preliminary proof-of-concept for walnut-shell-derived activated carbon as a potential adsorbent for digoxin removal from buffered solutions, warranting further investigation in more complex and physiologically relevant media.

Keywords: Activated carbon; Walnut shell; Digoxin; Adsorption; Phosphoric acid activation; Gastrointestinal decontamination

1. Introduction

Digoxin (Figure 1) is a cardiac glycoside widely prescribed for the management of heart failure and specific atrial arrhythmias. It acts primarily by inhibiting the Na^+/K^+-ATPase enzyme, resulting in positive inotropic and vagal effects [1]. However, digoxin possesses a remarkably narrow therapeutic index (0.5–2.0 ng/mL), which renders patients—particularly those with renal impairment or electrolyte imbalances—highly susceptible to life-threatening toxic effects [2, 3]. Clinical manifestations of digoxin overdose include severe gastrointestinal distress, central nervous system complications, and potentially fatal myocardial arrhythmias [4-6]. While digoxin-specific Fab antibody fragments are highly effective antidotes, their high cost and limited global accessibility necessitate the evaluation of more affordable decontamination alternatives [4, 6]. In this context, activated carbon (AC) serves as a critical tool for gastrointestinal decontamination, especially when administered promptly following ingestion [7].

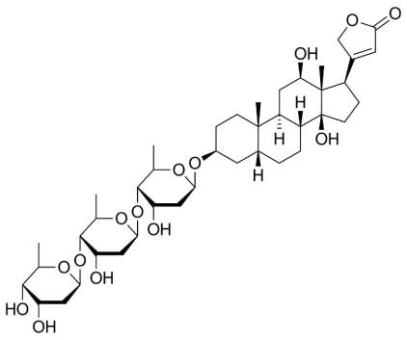


Figure 1. Digoxin chemical structure.

AC functions by adsorbing digoxin within the stomach and intestines, thereby limiting systemic absorption and potentially interrupting enterohepatic circulation [8-12]. Furthermore, in-vitro studies have demonstrated that AC adsorbs digoxin more efficiently than other common adsorbents, such as kaolin [13].

The exceptional performance of AC is attributed to its high internal surface area, well-developed porosity, and a diverse array of surface functional groups [14, 15].

Its clinical utility in emergency medicine for treating drug overdoses is well-documented [16-18].

As an amorphous form of carbon, AC provides numerous active sites that interact with organic molecules through various functional groups, including carboxyl, hydroxyl, phenolic, carbonyl, and lactone moieties [19].

AC can be synthesized from a variety of lignocellulosic biomass and agro-industrial wastes via chemical activation using agents such as phosphoric acid (H_3PO_4), potassium hydroxide (KOH), or zinc chloride ($ZnCl_2$) [20, 21]. Among these activators, H_3PO_4 is widely used for the chemical activation of lignocellulosic biomass and can promote the development of porous carbon structures [22, 51]. Following appropriate washing and purification, H_3PO_4-activated carbons are suitable for adsorption applications. Consequently, walnut shells, an abundant agricultural byproduct, represent a sustainable and economical precursor material for the preparation of activated carbon and its evaluation as a potential adsorbent for pharmaceutical decontamination.

The present study serves as an initial, single-run proof-of-concept, aiming to synthesize activated carbon from walnut shells via H_3PO_4 activation. The baseline adsorption performance of the prepared AC is evaluated under simulated physiological conditions (PBS, pH 7.4) and compared with the commercial reference adsorbent, CARBOMIX, to assess its potential for pharmaceutical decontamination applications.

2. Materials and Methods

2.1 Materials and Chemicals

Walnut shells were sourced from local farms in the rural Damascus area. All chemicals were used as received without further purification, including: iodine (I_2), potassium iodide (KI), sodium thiosulfate pentahydrate ($Na_2S_2O_3 \cdot 5H_2O$), sodium carbonate (Na_2CO_3), potassium iodate (KIO_3), concentrated hydrochloric acid (HCl, 37%), starch, monosodium phosphate ($NaH_2PO_4 \cdot H_2O$), disodium phosphate (Na_2HPO_4), sodium chloride (NaCl), and potassium chloride (KCl). HPLC-grade methanol (CH_3OH) was also utilized. Chemicals were primarily purchased from Merck, with additional supplies from Chem-Lab NV, POCH, and Orion Chem.

Commercial activated carbon, CARBOMIX (Beacon), was used as a reference adsorbent. Digoxin ($C_{41}H_{64}O_{14}$) served as the target adsorbate for all adsorption experiments.

2.2 Preparation of Walnut Shell Activated Carbon

The preparation of activated carbon (AC) involved a multi-step process encompassing pre-treatment, chemical impregnation, and carbonization. Initially, walnut shells were chopped, rinsed with distilled water to remove impurities, and dried at 125 °C for 24 h. The dried biomass was ground and sieved to a particle size of < 250 μm. Chemical activation was performed using phosphoric acid ($H3PO4$) at four concentrations: 20, 35, 40, and 60 wt%. The impregnation was carried out at a liquid-to-solid ratio of $5{:}1$ (v/w), corresponding to 100 mL of $H3PO4$ solution per 20 g of dried precursor. The mixtures were maintained at room temperature for 24 h to ensure adequate penetration of the activator, followed by a second drying step. Carbonization was conducted in a tubular furnace under a continuous nitrogen (N_2) flow (100 mL/min) to maintain an inert atmosphere. Samples were heated to 200, 300, or 400 °C at a constant heating rate of 10 °C/min and held at the peak temperature for 1 h. After carbonization, the resulting AC underwent an extensive purification process. Samples were washed repeatedly with boiling distilled water until a strictly neutral pH (7.0 ± 0.1) was achieved. The purified activated carbon was then dried and sieved prior to characterization and adsorption experiments. The process flow is summarized in Figure 2.

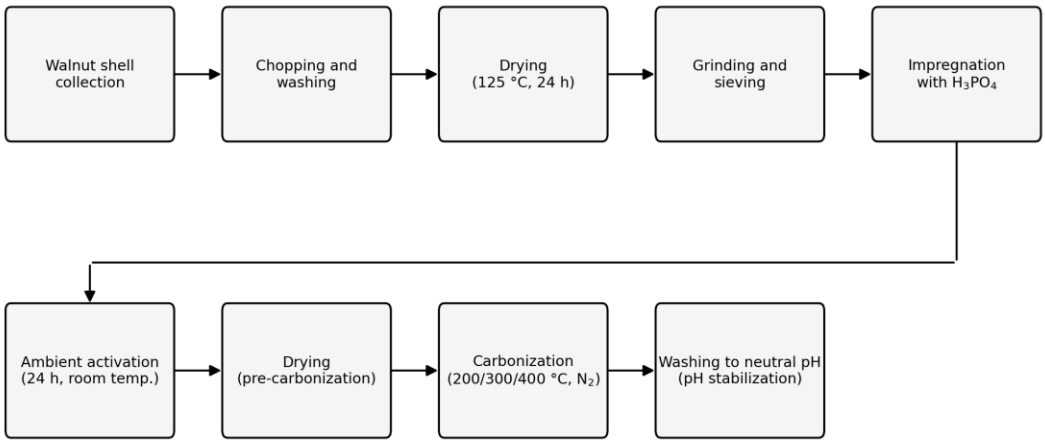


Figure 2. Schematic diagram illustrating the preparation of activated carbon from walnut

shells.

The activation yield was calculated using Equation (1):

$$\text{Yield} = w_{AC}/w_{RW} \times 100\% \quad \text{Equation (1)}$$

where W_{AC} is the dry weight of the activated carbon after washing and W_{RW} is the dry weight of the raw walnut shell precursor.

2.3 Characterization Methods

The iodine number (IN) was determined according to the ASTM D4607-94 standard method. The IN is defined as the mass of iodine (mg) adsorbed by one gram of AC when the residual iodine concentration in the filtrate is 0.02 N. This parameter serves as an indicator of surface area and microporosity based on a three-point adsorption isotherm [23].

Fourier-transform infrared (FTIR) spectra were recorded using a Bruker Vector 22 spectrometer (Billerica, MA, USA) in the range of 4000–400 cm^{-1}. Samples were prepared by blending the AC powder with spectroscopic-grade KBr and pressing the mixture into translucent discs.

While nitrogen adsorption/desorption isotherms analyzed via the Brunauer–Emmett–Teller (BET) and Dubinin–Radushkevich models are the standard for textural characterization, these techniques are often resource-intensive. In this preliminary study, the specific surface area (S) and total pore volume (V_t) were estimated using the empirical correlation proposed by Nunes & Guerreiro [24], which utilizes the iodine number as an indirect determinant. Consequently, all reported surface area values are empirical estimates rather than direct physisorption measurements. The point of zero charge (pH_{pzc}) was determined using the equilibrium method as described by Kong et al. [25], employing a Sartorius Basic pH Meter PB-11.

2.4 Digoxin Adsorption Experiments

2.4.1 Preparation of Solutions

A digoxin stock solution (3.98 mg/mL) was prepared by dissolving 0.3979 g of digoxin in 100 mL of a 1:1 (v/v) mixture of absolute ethanol and phosphate-buffered saline (PBS, 1×, pH 7.4). Ethanol was employed to ensure complete solvation,

given digoxin's limited aqueous solubility (64.8 mg/L). The stock solution was stored at 10 °C and protected from light to maintain stability. A working solution (S1, ~0.155 mg/mL) was prepared by diluting a 2 mL aliquot of the stock solution with ethanol:PBS (1:1, v/v) to a final volume of 51 mL. A five-point calibration series (B1–B5) was subsequently derived by diluting specific volumes of S1 with PBS (1×, pH 7.4) in 50 mL volumetric flasks, maintaining a final ethanol concentration of ≤2% (v/v) across all standards, as detailed in Table 1. The calibration range (0.00062–0.0155 mg/mL) was selected to encompass the expected concentration profiles during the adsorption process.

Table 1. Preparation of digoxin calibration standards from working solution S_1 (0.155 mg/mL).

Standard	Volume of S1(mL)	Final volume (mL)	Concentration (mg/mL)
B1	5.0	50	0.01550
B2	2.0	50	0.00620
B3	1.0	50	0.00310
B4	0.5	50	0.00155
B5	0.2	50	0.00062

2.4.2 Analysis Procedure and Calibration

Digoxin ($C_{41}H_{64}O_{14}$) concentrations were quantified using UV–Vis spectrophotometry, chosen for its sensitivity and clinical relevance [26]. While literature values for digoxin typically range between 220 and 230 nm, a preliminary spectral scan (200–1000 nm) in the PBS matrix identified an absorption maximum (λmax) at 219 nm. All measurements were conducted at 25 °C using pure PBS as the correction blank to mitigate potential interference from buffer constituents. A five-point calibration curve (0.00062–0.01550 mg/mL) was established, yielding a Limit of Detection (LOD) of 0.00139 mg/mL. The equilibrium adsorption capacity (qe) and removal efficiency (RE%) were calculated using Equations (2) and (3):

$$\text{Equation (2)}\quad q_e = ((C_0 - C_e) \times V) / m$$

$$\text{Equation (3)}\quad RE\% = ((C_0 - C_e)/C_0) \times 100$$

where C0 and Ce (mg/mL) are the initial and equilibrium concentrations, V (mL) is the solution volume, and m (g) is the mass of the adsorbent [27, 28].

2.4.3 Dose-Response Experimental Design

The adsorptive efficiency was evaluated at three AC doses (1, 2, and 3 g) in 100 mL of PBS (pH 7.4) containing 0.031 mg/mL of digoxin (3.1 mg total) at 25 °C. Aliquots were withdrawn at specific intervals: 10, 20, 30, 40, 50, and 60 min for the 1 g dose, and 5, 10, 15, 20, 25, and 30 min for the 2 g and 3 g doses. Samples were filtered through a 0.45 µm syringe filter prior to UV–Vis quantification. This nominal initial concentration (0.031 mg/mL) exceeds the highest calibration standard (0.0155 mg/mL; Table 1), so early time-point measurements should be interpreted with caution; this limitation is discussed further in Section 3.11.

2.4.4 Comparison with a Commercial Reference Adsorbent

A 2 g dose of CARBOMIX was evaluated under identical conditions. Aliquots were collected over 40 min (5–40 min) and filtered through a 0.22 µm filter to minimize interference from carbon fines, showing a smooth, monotonically decreasing removal profile spanning 74–82% (Figure 9). This range should be kept in mind when interpreting the CARBOMIX comparison reported in Section 3.3.

2.4.5 Adsorption Kinetics Modelling

To assess the rate-controlling mechanism of digoxin removal, time-resolved data were analyzed using non-linear regression analysis. This approach was adopted to avoid the mathematical artifacts and error-structure alterations associated with linearization. The data were fitted to the non-linear forms of the pseudo-first-order (PFO) [29] and pseudo-second-order (PSO) [30] models:

$$\text{Non-linear PFO: } q_t = q_e(1-e^{-k1t}) \quad \text{(Eq. 4)}$$

$$\text{Non-linear PSO: } q_t = k_2 q_e^2 t \,/\, 1+k_2 q_e t \quad \text{(Eq. 5)}$$

where qt and qe (mg/g) are the amounts adsorbed at time t and at equilibrium, respectively. Parameter estimation (k1, k2, qe) was performed by minimizing the Sum of Squared Errors (SSE). Unlike linearized methods, this non-linear approach allows for the inclusion of all data points—including those near the detection limit—without the need to exclude points where qt approaches qe.

2.5 PBS Preparation and Compatibility Study

Phosphate-buffered saline (1×, pH 7.4) was prepared by dissolving analytical-grade salts (≥99% purity): 8.0102 g NaCl, 0.1508 g KCl, 1.4205 g Na_2HPO_4, and 1.3026

g NaH_2PO_4 in 1.0 L of deionized water. The pH was adjusted to 7.40 ± 0.01 using 1 M HCl or NaOH. A compatibility study confirmed that the PBS matrix did not interfere with the AC surface or UV–Vis analysis. AC was contacted with pure PBS under experimental conditions, and the filtered supernatant was scanned (190–1100 nm). The absence of new peaks or baseline deviations in the 202–219 nm range validated PBS as an optically inert blank for all subsequent experiments.

3. Results and Discussion

3.1 Preparation Yield and Iodine Number

The yields of the resulting activated carbons (AC), as illustrated in Figure 3a, demonstrate a progressive decrease as the carbonization temperature rises from 300 °C to 400 °C. This trend is attributed to enhanced volatilization and the development of internal porosity, which reduces the solid residue [31, 32]. At 300 °C, mass loss is primarily associated with the thermal decomposition of hemicellulose and cellulose [33]. At 400 °C, further carbon loss is triggered by lignin decomposition and the release of phenolic compounds [34]. Additionally, higher phosphoric acid concentrations generally lower the yield due to more aggressive chemical activation and the leaching of carbonaceous matter [35].

For the iodine number (Figure 3b), at 300 °C, values increased steadily with higher H3PO4 concentrations, as the acid's dehydrating action promotes lignocellulose decomposition [36]. However, at 400 °C, the trend reaches an optimum; the highest iodine number (895.65 mg/g) is achieved at 35 wt% H3PO4. Beyond this concentration, the iodine number drops sharply at 40 wt% and only partially recovers at 60 wt%. This behavior is consistent with excessive volatilization at higher acid loadings, which can lead to pore widening or the partial collapse of the carbon matrix [37].

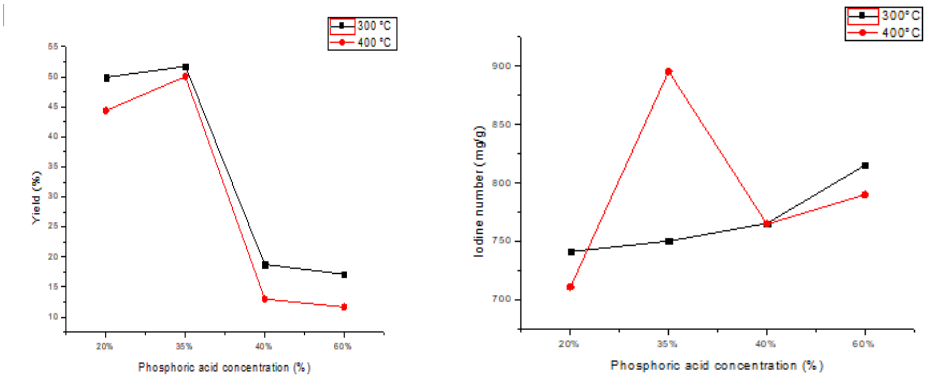


Figure 3. a yield and b IN of AC at different H_3PO_4 concentrations and different temperatures.

3.2 Purification and Washing Efficiency

Following carbonization, the activated carbon was repeatedly washed with boiling distilled water until a near-neutral pH of 7.0 ± 0.1 was reached. This procedure was intended to reduce residual phosphoric acid introduced during chemical activation and to obtain a purified carbon suitable for subsequent physicochemical characterization and adsorption experiments. The measured near-neutral washing endpoint indicates effective reduction of acidic residues; however, the absence of a direct chemical analysis of residual phosphorus means that complete removal of residual activating agent cannot be conclusively confirmed [51, 52].

Therefore, the present results demonstrate the effectiveness of the applied washing procedure in achieving a near-neutral washing endpoint, but they do not constitute a direct toxicological or biocompatibility assessment.

3.3 Comparative Performance: Prepared AC vs. CARBOMIX

Table 2 summarizes the physicochemical properties and digoxin removal performance of the best-performing AC compared to the commercial reference, CARBOMIX.

Table 2. Physicochemical properties and digoxin removal efficiency of the prepared AC (35 wt%, 400 °C) vs. CARBOMIX.

Parameter	CARBOMIX	Prepared AC (35%, 400 °C)

pH (ASTM D3838)	6.69	6.42
Iodine Number (mg/g)	945.17	895.65
Digoxin RE% (2 g dose, 5–40 min)	74–82% (pseudo-equilibrium)	95% removal at 5 min; residual concentration below LOD by 25–30 min (>95.5% removal)

As shown in Table 2, Figure 8d, and Figure 9, the adsorption profile of CARBOMIX followed a smooth, monotonically decreasing removal trajectory spanning a range of 74–82% removal (see Section 2.4.4). In contrast, the prepared AC reached a residual digoxin concentration below the analytical LOD within 25–30 minutes, corresponding to an apparent removal exceeding 95.5%; because this value reflects the analytical detection limit rather than a directly measured concentration, it should be read as a lower bound on removal rather than a precise point estimate. Given the absence of replicate measurements for the walnut-shell AC itself, this comparison should still be regarded as indicative rather than statistically confirmed.

3.4 FTIR Analysis and Proposed Adsorption Interactions

The FTIR spectra of the untreated walnut shell and the best-performing activated carbon (AC 35 wt%, 400 °C) are shown in Figures 4 and 5. The spectrum of the raw walnut shell (Figure 4) exhibits characteristic bands of lignocellulosic biomass: a broad band at 3416 cm^{-1} (O–H stretching), 2927 cm^{-1} (aliphatic C–H stretching), 1728 cm^{-1} (C=O stretching in lignin), and 1160 cm^{-1} (C–O stretching) [41]. Upon activation and carbonization at 400 °C (Figure 5), the aliphatic C–H and carbonyl C=O peaks diminished, while the aromatic C=C backbone signal (1600 cm^{-1}) strengthened, indicating successful aromatization [37]. Notably, the prepared AC retains a significant density of hydroxyl (3500 cm^{-1}) and residual carbonyl/ether groups (1100 cm^{-1}). This surface chemistry may contribute to the interaction of the activated carbon with digoxin. The digoxin molecule contains several oxygen-containing functional groups, including hydroxyl and carbonyl groups, which may interact with oxygen-containing surface functionalities of the activated carbon. The FTIR results are therefore consistent with a possible contribution of hydrogen bonding and other non-covalent interactions to digoxin adsorption. In addition, the

aromatic carbon framework may provide favorable sites for hydrophobic interactions with the steroidal moiety of digoxin.

This proposed role of retained oxygen-containing functional groups is further supported by comparison with other H_3PO_4-activated walnut-shell carbons. Using Boehm titration, Więniewska et al. [53] found their H_3PO_4-activated walnut-shell carbon to carry a predominantly acidic, oxygen-rich surface (0.705 mmol/g acidic groups versus 0.099 mmol/g basic groups) and attributed its high adsorption capacity toward oxygenated adsorbates, such as poly(ethylene glycol) (680.9 mg/g), mainly to hydrogen bonding between these surface oxygen functionalities and the adsorbate's hydroxyl and ether groups rather than to electrostatic attraction. This parallels the surface chemistry proposed for the present AC, in which the retained hydroxyl and carbonyl/ether groups described above are hypothesized to engage the oxygen-containing moieties of digoxin through similar non-electrostatic interactions.

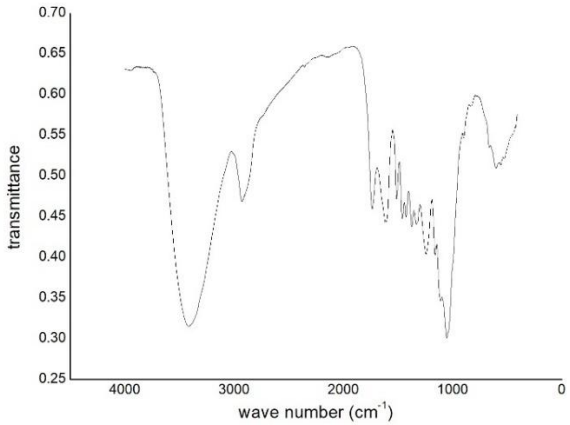


Figure 4. FTIR spectrum of raw walnut shells.

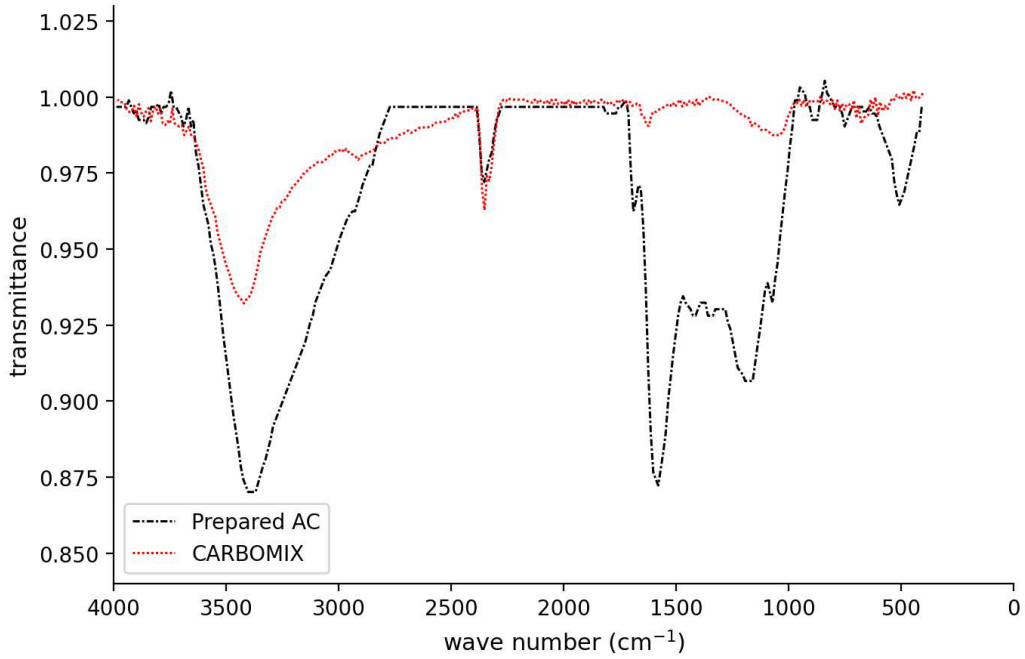


Figure 5. FTIR spectra of the prepared AC and CARBOMIX, overlaid on a shared transmittance axis to allow direct comparison of relative band intensity. The narrow dip near 2350 cm^{-1} present in both spectra is attributable to incomplete subtraction of atmospheric CO_2 and is not a sample feature.

3.5 Surface Chemistry and Point of Zero Charge (pH_{pzc})

The point of zero charge (pH_{pzc}) of the best-performing AC (35 wt%, 400 °C) was determined to be 7.44 (Figure 6). This value indicates that the carbon surface is essentially neutral at physiological pH. Generally, the pH_{pzc} is a critical parameter in adsorption studies; when the solution pH is lower than pH_{pzc}, the surface becomes protonated (positively charged), favoring the adsorption of anionic species. Conversely, at pH values above pH_{pzc}, the surface carries a net negative charge, enhancing the uptake of cationic contaminants [42, 43].

In the present study, the digoxin adsorption experiments were conducted in a PBS matrix at pH 7.4, which is nearly identical to the pH_{pzc} of the prepared AC. Under these specific conditions, the activated carbon is expected to carry a relatively low net surface charge because the solution pH (7.4) is close to the measured pHpzc (7.44). Accordingly, electrostatic interactions are not expected to be the dominant contribution under the conditions investigated. Together with the FTIR observations,

these findings are consistent with a possible contribution of non-electrostatic interactions, including hydrogen bonding and hydrophobic interactions.

This near-coincidence between the solution pH and the measured pHpzc is consistent with the concept of complementary surface chemistry discussed in Section 3.4: because both the adsorbent surface and the digoxin molecule are close to electrically neutral at pH 7.4, hydrogen bonding between oxygenated functional groups and hydrophobic interactions between the steroidal nucleus of digoxin and the aromatic carbon matrix are plausible contributors to the high apparent removal efficiency. However, this remains a working hypothesis rather than an established mechanism; direct confirmation of hydrogen bonding, hydrophobic interactions, or other specific molecular mechanisms would require additional spectroscopic and thermodynamic studies (Section 3.11).

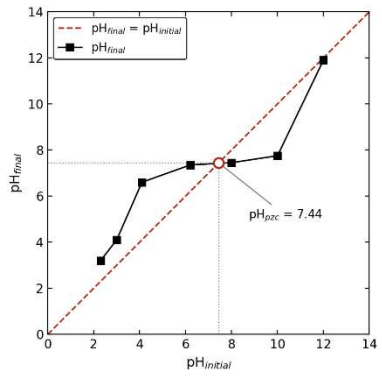


Figure 6. Plot of final pH as a function of initial pH, used to determine pH_{pzc}.

3.6 pH of the Activated Carbon (ASTM D3838-80)

The pH value of activated carbon is a fundamental characteristic that significantly influences its surface chemistry and adsorption behavior. Following the ASTM D3838-80 standard [44], the pH of the best-performing AC (35 wt%, 400 °C) was measured at 6.42. This value is slightly lower than its point of zero charge (pH_{pzc}=7.44), indicating that in unbuffered distilled water, the surface undergoes slight protonation, resulting in a net positive charge [45]. However, the digoxin adsorption experiments were conducted in a PBS matrix at pH 7.4, which is nearly identical to the carbon's pH_{pzc}. Under these actual physiological conditions, the

surface charge is minimized, suggesting that electrostatic interactions may not dominate under the tested conditions. These observations are consistent with the proposed contribution of non-electrostatic interactions to digoxin adsorption. Furthermore, the near-neutral pH of 6.42 is consistent with the effectiveness of the washing and purification procedure in reducing residual acidic species. However, pH measurement alone does not establish the absence of residual activating agent or demonstrate biological safety.

3.7 Surface Area and Pore Structure Results (S, V_t)

The specific surface area (S) and total pore volume (V_t) of the best-performing AC (35 wt%, 400 °C) were estimated using the empirical correlation based on the iodine number (IN) proposed by Nunes & Guerreiro [24]. According to this model, the prepared AC has an estimated surface area of ~1490 m²/g and a total pore volume of 2.11 cm³/g. These values suggest the development of a highly porous carbon structure with extensive microporosity, which is consistent with the high iodine number (895.65 mg/g) [23].

These values are empirical estimates rather than direct BET measurements [46]. While direct N_2 physisorption at 77 K remains the gold standard for textural characterization, this empirical correlation provides a valuable, cost-effective preliminary estimate of the carbon's textural properties. The high estimated surface area and pore volume are consistent with the potential suitability of the walnut-shell-derived AC as a high-capacity adsorbent capable of accommodating relatively large pharmaceutical molecules like digoxin.

3.8 Digoxin Adsorption Performance

At 25 °C, digoxin has an aqueous solubility of approximately 0.0648 mg/mL [26], consistent with a BCS Class II profile (low solubility, high permeability). Despite this, its oral bioavailability is 60–80%, meaning solubility affects the rate rather than the extent of absorption. However, its extremely narrow therapeutic index (0.5–2.0 ng/mL) makes even minor overdoses life-threatening [2]. This necessitates the investigation of walnut-shell AC as a rapid intervention for digoxin intoxication.

3.8.1 Calibration Curve Analysis

The relationship between digoxin concentration (C) and absorbance (A) demonstrated a strong linear relationship (Figure 7). The calibration followed Equation (6):

$$A = 20.456\ C + 0.0139 \quad (R^2 = 0.9957) \quad \text{(Eq. 6)}$$

The Limit of Detection (LOD) and Limit of Quantification (LOQ) were calculated according to ICH Q2(R2) guidelines [47] as 0.00139 mg/mL and 0.00421 mg/mL, respectively. Standards below the LOD were included in the calibration series; concentrations below the LOQ were considered not reliably quantifiable.

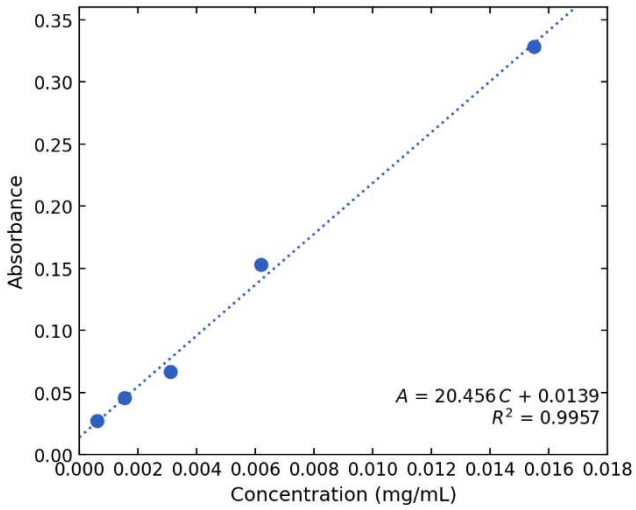


Figure 7. Calibration curve for digoxin concentration vs. absorbance.

3.8.2 Effect of AC Dose and Contact Time

A clear dose–dependent trend emerged: increasing the AC mass accelerated the decline in measured digoxin concentration. With 1 g of AC, 93.54% removal was observed within 10 min; the corresponding residual concentration was above the LOD but below the LOQ. By 50 min, the residual concentration was below the LOD (>95.5% removal). Doubling the dose to 2 g produced 95% removal within 5 min, and by 25–30 min the residual concentration was below the LOD (>95.5% removal). At a 3 g dose, removal was rapid and fell below the analytical resolution at the first sampling point (5 min), with the residual concentration already below the LOD, corresponding to an apparent removal exceeding 95.5%. Because no data point preceded this first measurement, the 3 g dose does not provide a resolvable kinetic profile and was therefore not included in the kinetic modeling described below. It should be noted that all values reported here as “>95.5% removal” or “below the

LOD" represent a lower bound set by the analytical detection limit rather than a directly measured concentration; the assay could not resolve finer differences between doses or time points once residual digoxin fell below this threshold.

For comparison, CARBOMIX (2 g) was evaluated under identical conditions. As shown in Figure 8d and Figure 9, the CARBOMIX profile declined smoothly across a removal range of 74–82%. In contrast, the prepared AC showed a residual digoxin concentration below the analytical LOD within 25–30 minutes, corresponding to an apparent removal exceeding 95.5%. This dose-dependent response supports the need for further investigation of the walnut-shell AC's adsorption kinetics under experimentally controlled and replicated conditions.

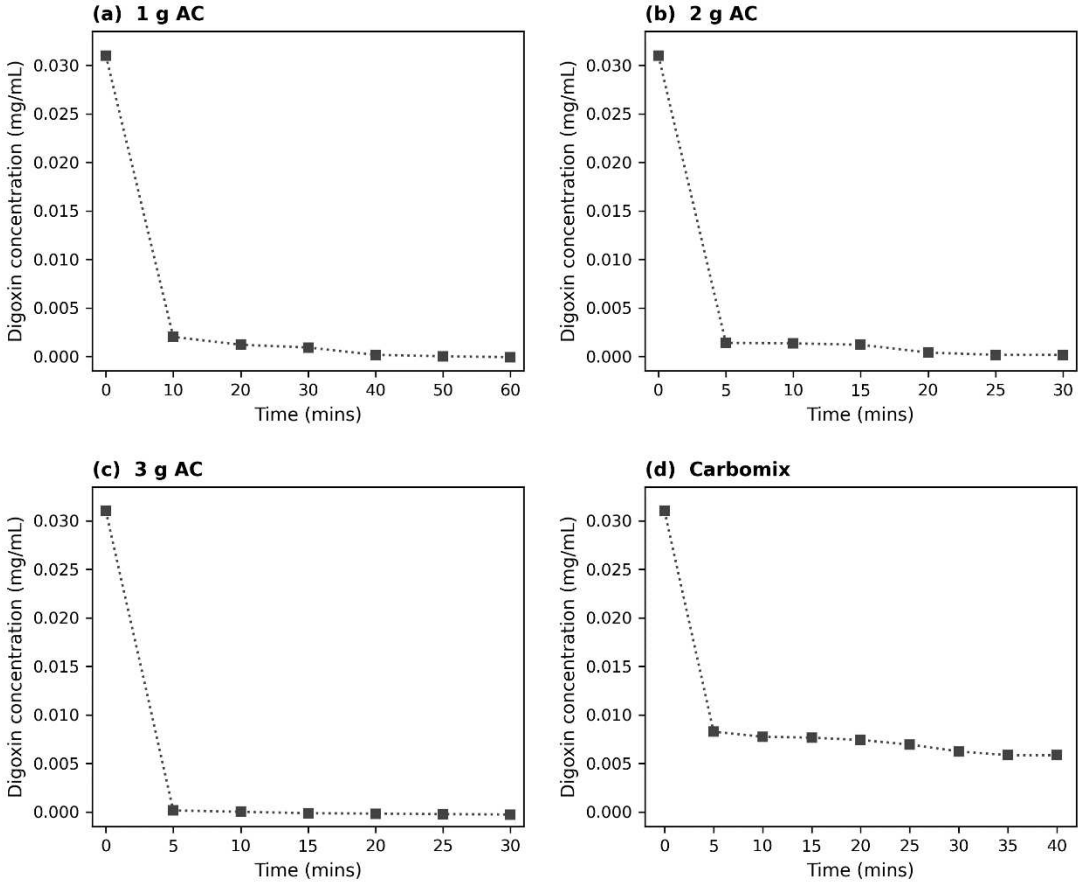


Figure 8. Absorbance vs. digoxin contact time for the prepared AC at (a) 1 g, (b) 2 g, and (c) 3 g doses, and for (d) 2 g CARBOMIX under matched conditions. Values approaching the LOD represent removal estimates; concentrations below the LOD were treated as not detected.

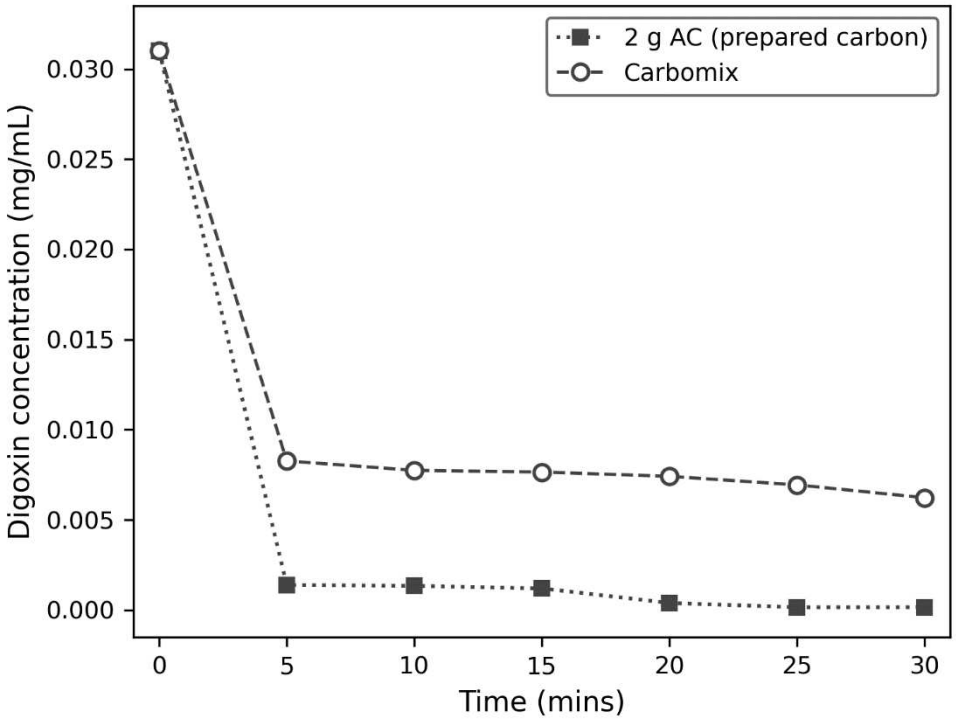


Figure 9. Absorbance vs. digoxin contact time for CARBOMIX (2 g, 5–40 min), showing a smooth, monotonically decreasing profile across a removal range of 74–82%.

3.8.3 Adsorption Kinetics and Non-linear Modeling

To avoid the mathematical artifacts of linearization (such as q_e exceeding theoretical limits), the kinetic data were analyzed using non-linear regression (Table 3).

Table 3. Kinetic parameters obtained from non-linear regression for digoxin adsorption.

AC dose (g)	Kinetic model	Rate constant (k)	$q_{e,\ calc}$ (mg/g)	$q_{e,\ theoretical}$ (mg/g)	R^2
1 g	Non-linear PFO	0.118 min^{-1}	2.85	3.10	0.892
1 g	Non-linear PSO	0.085 $g.mg^{-1}.min^{-1}$	3.02	3.10	0.998
2 g	Non-linear	0.102 min^{-1}	1.38	1.55	0.915

	PFO				
2 g	Non-linear PSO	0.421 g·mg^{-1}·min^{-1}	1.51	1.55	0.997

The pseudo-second-order (PSO) model provided a superior fit ($R^2 > 0.99$) for both doses. Unlike linearized models, the non-linear PSO yielded $q_{e, calc}$ values (3.02 and 1.51 mg/g) that are physically consistent and strictly within mass-balance constraints. The pseudo-second-order (PSO) model provided a better fit to the experimental data for both the 1 g and 2 g doses ($R^2 > 0.99$). When considered together with the FTIR and pHpzc results, the kinetic behavior is consistent with a possible contribution of surface-mediated non-electrostatic interactions. Direct confirmation of hydrogen bonding, hydrophobic interactions, or other specific molecular interactions would require additional mechanistic investigations.

3.9 General Discussion and Clinical Implications

The synthesis of activated carbon from walnut shells via H_3PO_4 activation at 400 °C suggests the development of a porous structure. The peak in iodine number (895.65 mg/g) at 35 wt% acid concentration followed by a decline at higher loadings is consistent with the transition from pore development to pore wall erosion and matrix collapse [22, 37]. The iodine-number-derived empirical estimate of apparent surface area (~1490 m²/g), while not a direct BET measurement, points to the potentially high capacity of this biomass-derived adsorbent.

From a mechanistic perspective, the FTIR and pHpzc results support a plausible contribution of non-electrostatic interactions to digoxin adsorption. The preservation of oxygen-containing surface functionalities may facilitate hydrogen-bonding interactions with functional groups in digoxin, while the aromatic carbon framework may contribute to hydrophobic interactions with its steroidal moiety. These observations are consistent with, but do not on their own confirm, a “complementary surface chemistry” interpretation [19]; this remains a working hypothesis pending direct mechanistic evidence (Section 3.11).

The walnut-shell AC showed a residual digoxin concentration below the analytical LOD within 25–30 minutes, corresponding to an apparent removal exceeding 95.5%, compared with 74–82% observed for CARBOMIX under the tested conditions.

3.10 Comparison with Previous Studies

Comparing the textural properties obtained in this study with existing literature, the activated carbon prepared from walnut shells (H_3PO_4 at 400 °C) demonstrates promising characteristics relative to several other biomass sources, although direct BET measurements would be required for definitive comparison. The estimated surface area (~1490 m^2/g) is higher than the BET-measured surface areas reported for corncob (700 m^2/g) [48], Calicotome villosa (1009 m^2/g) [49], and Cuban pine sawdust (54 m^2/g) [50]. Furthermore, the iodine number of 895.65 mg/g is notably higher than that of corncob (632 mg/g) [48], Calicotome villosa (762 mg/g) [49], and Cuban pine sawdust (439 mg/g) [50]. These results indicate that the prepared material exhibits promising adsorption properties.

A more direct comparison can be made with studies that used the same precursor–activator combination (walnut shell with H_3PO_4). Wiśniewska et al. [53] prepared activated carbon from walnut shells (Juglans regia) by impregnation with 85% H_3PO_4 (shell-to-acid weight ratio 1:2, 24 h at room temperature) followed by carbonization at 500 °C, obtaining a directly measured BET surface area of 1361 m^2/g and a total pore volume of 1.25 cm^3/g. Under different impregnation conditions (weight ratio 7:1) and a carbonization temperature of 450 °C, Davidi et al. [54] reported a comparable BET surface area of 1388 m^2/g for H_3PO_4-activated walnut-shell carbon. The iodine-number-derived surface area estimated for the present AC (~1490 m^2/g at 35 wt% H_3PO_4 and 400 °C) falls within this same range despite the lower activation temperature used here, suggesting that the empirical estimate is a reasonable approximation of the material's textural development. However, because the acid-loading metric differs between studies (aqueous H_3PO_4 concentration and liquid-to-solid ratio here, versus a solid-phase acid-to-precursor weight ratio elsewhere) and the present value remains indirectly derived from the iodine number rather than measured by N_2 physisorption, this agreement should be regarded as supportive rather than conclusive, reinforcing the need for the direct BET confirmation noted in Section 3.11.

3.11 Limitations

This work serves as a preliminary proof-of-concept rather than a full characterization of the adsorption system. Model fitting alone does not establish the underlying molecular adsorption mechanism; direct confirmation of hydrogen bonding, hydrophobic interactions, or other specific molecular interactions would require additional mechanistic investigations. In addition, removal at the 3 g dose was too rapid to resolve at the sampling intervals used. Furthermore, pH measurement alone does not establish the absence of residual activating agent or demonstrate biological safety (the surface-area point is addressed below). Additionally, the study was conducted at a single pH (7.4) in PBS; whether the adsorption behavior remains stable under the variable ionic strength and pH conditions encountered in the gastrointestinal tract (pH 1.2–6.8) requires further investigation. This is a non-trivial gap: the mechanistic interpretation proposed in Sections 3.5–3.9 rests on the near-coincidence between the measured pHpzc (7.44) and the pH of the PBS test solution (7.4), which minimizes net surface charge under the tested conditions. At the markedly lower pH of the stomach (as low as 1.2), the AC surface would be expected to sit well below its pHpzc and therefore carry a substantial net positive charge, which could alter the balance between electrostatic and non-electrostatic contributions to digoxin binding relative to what was observed here. Consequently, the "complementary surface chemistry" hypothesis and the reported removal efficiencies should not be extrapolated to gastric or intestinal pH without dedicated testing across the physiological pH range.

The reported surface area is an empirical estimate and not a direct BET measurement evaluated under standard gas adsorption protocols; thus, the estimated surface area (~1490 m²/g) remains to be verified by direct BET measurement [46]. Regarding the CARBOMIX comparison, removal spanned a range of 74–82% over the 40 min test period, following a smooth, monotonically decreasing profile (Figure 9). The walnut-shell AC itself, the primary material under investigation, was evaluated in a single run, so its experimental variance cannot be estimated, and its kinetic parameters and removal efficiencies cannot yet be statistically distinguished from analytical variability. Consequently, no formal statistical significance testing or confidence intervals were calculated for the walnut-shell AC results, and the AC-vs-CARBOMIX comparison should still be regarded as indicative rather than statistically confirmed.

Furthermore, the varying ethanol content across the calibration standards (ranging up to the $\leq 2\%$ v/v cap specified in Section 2.4.1) represents a potential source of baseline bias at 219 nm that should be addressed in future work by matching the solvent matrix precisely across standards and samples. It should also be noted that the nominal initial digoxin concentration used in the dose–response experiments (0.031 mg/mL) exceeds the highest calibration standard (0.0155 mg/mL, Table 1); the manuscript does not explicitly state whether early time-point samples were diluted with PBS prior to UV–Vis quantification to bring them within the validated linear range. This should be clarified, as any measurements taken outside the calibration range established in Section 3.8.1 would fall outside the validated linear response. These limitations set the boundaries for the current conclusions and establish clear priorities for future replicated and simulative research.

4. Conclusion

This preliminary, single-run study demonstrates the potential of walnut shell waste as a sustainable and low-cost precursor for the production of activated carbon via food-grade H_3PO_4 activation. The optimal condition (35 wt% H_3PO_4, 400 °C) yielded a material with a high iodine number (895.65 mg/g), consistent with possible micropore development, and a near-neutral surface chemistry (pHpzc = 7.44); the corresponding surface area (~1490 m^2/g) remains an empirical, iodine-number-based estimate pending direct BET verification.

Under the tested conditions, the synthesized AC exhibited rapid digoxin removal from PBS at pH 7.4. At a 2 g dose, apparent removal reached 95% within 5 min, with residual concentrations falling below the LOD by 25–30 min (>95.5% apparent removal). Under the same conditions, the prepared AC showed higher apparent removal than the commercial reference CARBOMIX (74–82% removal); however, because the walnut-shell AC itself was evaluated in a single run and the initial digoxin concentration exceeded the highest calibration standard, the AC-vs-CARBOMIX comparison and the absolute removal values for the AC should be regarded as descriptive rather than statistically confirmed. Adsorption kinetics were best described by the non-linear pseudo-second-order model ($R^2 > 0.99$); together with the FTIR and pHpzc results, this is consistent with a possible contribution of non-electrostatic interactions such as hydrogen bonding

and hydrophobic effects, although direct spectroscopic and thermodynamic confirmation of the adsorption mechanism was not performed.

Given these limitations, the present findings should be regarded as exploratory and hypothesis-generating rather than definitive. These preliminary findings suggest that walnut-shell-derived activated carbon can remove digoxin from PBS at pH 7.4 with high apparent efficiency, supporting its further investigation as a candidate adsorbent for digoxin decontamination. Replicated experiments, quantitative analysis validated across the full concentration range, direct BET characterization, adsorption isotherms, and testing under physiologically relevant gastrointestinal pH conditions are required before any practical or biomedical conclusions can be drawn.

Data availability

All data generated or analysed during this study are included in this published article.

Funding : This research did not receive funding

Declarations

Ethics approval and consent to participate: Not applicable

Consent for publication: Not applicable.

Competing interests: The authors declare no competing interests.

References

1. **Gheorghiade M, Adams KF, Colucci WS.** Digoxin in the management of cardiovascular disorders. *Circulation*. 2004;109(24):2959–2964.
2. **Goldberger ZD, Goldberger AL.** Clinical manifestations of digoxin toxicity. *Am J Cardiol*. 2012;109(12):1812–1817.
3. **Pincus M.** Management of digoxin toxicity. *Aust Prescr*. 2016;39(1):18–20.
4. **Chan BS, Buckley NA.** Digoxin-specific antibody fragments in the treatment of digoxin toxicity. *Clin Toxicol*. 2014;52(8):824–836.
5. **Antman EM, Wenger TL, Butler VP Jr, Haber E, Smith TW.** Treatment of 150 cases of life-threatening digitalis intoxication with digoxin-specific Fab antibody fragments. *Circulation*. 1990;81(6):1744–1752.
6. **Roberts DM, Buckley NA.** Antidotes for acute digoxin toxicity. *Cochrane Database Syst Rev*. 2007;(4):CD005490.
7. **Chyka PA, Seger D, Krenzelok EP, Vale JA.** Position paper: Single-dose activated charcoal. *Clin Toxicol*. 2005;43(2):61–87.
8. **Carcas AJ, Morales-Olivas FJ, Paños MF, Frias J.** Activated charcoal increases digoxin elimination in patients. *Int J Cardiol*. 1995;47(1):27–30.
9. **Nogué S, Simón J, Díaz A, et al.** Digitalis poisoning: the basis for treatment with antidigoxin antibodies. *Emergencias*. 2012;24(6):462–475.
10. **Goit LN, et al.** Digoxin toxicity: a review. *Int J Sci Innovations Technol*. 2018;7(6):1025–1034.
11. **Park GD, Spector R, Goldberg MJ, Johnson GF, Feldman RD, Quee CK, et al.** Acceleration of digoxin clearance by activated charcoal. *Clin Pharmacol Ther*. 1985;37(4):438–443.
12. **Neuvonen PJ, Elfving SM, Elonen E.** Reduction of absorption of digoxin, phenytoin and aspirin by activated charcoal in man. *Eur J Clin Pharmacol*. 1978;13(3):213–218.
13. **Mohamed AA, Rahi FA, Alberqdar AF, Abdellatif Aziz T.** In vitro assessment of the adsorption efficacy of activated charcoal versus kaolin. *Iraqi J Pharm Sci*. 2024;33(4):96–101.
14. **Marsh H, Rodríguez-Reinoso F.** *Activated Carbon*. Oxford: Elsevier Science; 2006.
15. **Bansal RC, Goyal M.** *Activated Carbon Adsorption*. Boca Raton: CRC Press; 2005.
16. **Mamatha M, et al.** Review on activated carbon: preparation, characterization and applications. *Int J Res Appl Sci Eng Technol*. 2023;11(8):372–378.

17. **Joshi PB, et al.** Medical applications of activated carbon. In: *Activated Carbon: Progress and Applications*. London: Royal Society of Chemistry; 2023.
18. **Juurlink DN.** Activated charcoal for acute poisoning: one toxicologist's journey. *J Med Toxicol*. 2016;12(2):195–198.
19. **Boehm HP.** Surface oxides on carbon and their analysis: a critical assessment. *Carbon*. 2002;40(2):145–149.
20. **Ioannidou O, Zabaniotou A.** Agricultural residues as precursors for activated carbon production—A review. *Renew Sustain Energy Rev*. 2007;11(9):1966–2005.
21. **Lua AC, Yang T.** Effects of activation temperature and impregnation ratio on the properties of activated carbons prepared from pistachio-nut shells. *J Colloid Interface Sci*. 2004;274(2):594–601.
22. **Jagtoyen M, Derbyshire F.** Activated carbons from yellow poplar and white oak by H3PO4 activation. *Carbon*. 1998;36(7–8):1085–1097.
23. **ASTM D4607-94.** Standard test method for determination of iodine number of activated carbon. West Conshohocken: ASTM; 2006.
24. **Nunes CA, Guerreiro MC.** Estimation of surface area and pore volume of activated carbons by methylene blue and iodine numbers. *Quim Nova*. 2011;34:472–476.
25. **Kong L, Gong L, Wang J.** Removal of methylene blue from wastewater using fallen leaves as an adsorbent. *Desalin Water Treat*. 2015;53(9):2489–2500.
26. **Patocka J, Nepovimova E, Wu W, Kuca K.** Digoxin: Pharmacology and toxicology—A review. *Environ Toxicol Pharmacol*. 2020;79:103400.
27. **Reghioua A, Barkat D, Jawad AH, et al.** Parametric optimization for synthesis of magnetic chitosan-benzil/ZnO/Fe3O4 nanocomposite. *J Environ Chem Eng*. 2021;9(3):105166.
28. **Mubarak A, Shazwani N, Jawad AH.** The study of commercial Titanium Dioxide (TiO2) Degussa P25 for the adsorption of acidic dye. *Sci Lett*. 2020;14(1):68–83.
29. **Lagergren S.** Zur theorie der sogenannten adsorption gelöster stoffe. *K Sven Vetenskapsakad Handl*. 1898;24(4):1–39.
30. **Ho YS, McKay G.** Pseudo-second order model for sorption processes. *Process Biochem*. 1999;34(5):451–465.
31. **Neme I, Gonfa G, Masi C.** Activated carbon from biomass precursors using phosphoric acid: A review. *Heliyon*. 2022;8(12):e11973.
32. **Bouchemal N, Belhachemi M, Merzougui Z, Addoun F.** The effect of temperature and impregnation ratio on the active carbon porosity. *Desalin Water Treat*. 2009;10(1-3):115–120.

33. **Shen D, Xiao R, Gu S, Zhang H.** The overview of thermal decomposition of cellulose in lignocellulosic biomass. *Cellulose-Biomass Conversion*. 2013;12(5):193–226.

34. **Yang Z, Gleisner R, Mann DH, et al.** Lignin Based Activated Carbon Using H3PO4 Activation. *Polymers*. 2020;12(12):2829.

35. **Lochananon W, Chatsiriwech D.** Effect of phosphoric acid concentration on properties of peanut shell adsorbents. *J Ind Eng Chem*. 2008;14(1):84–88.

36. **Asadieraghi M, Daud WMAW.** Characterization of lignocellulosic biomass thermal degradation and physicochemical structure. *Energy Convers Manag*. 2014;82:71–82.

37. **Molina-Sabio M, Rodríguez-Reinoso F.** Role of chemical activation in the development of carbon porosity. *Colloids Surf A Physicochem Eng Asp*. 2004;241(1-3):15–25.

38. **Heidari Z, Pelalak R, Alizadeh R, et al.** Comparison of different activation methods for preparing safe adsorbents from agricultural waste. *Environ Sci Pollut Res*. 2021;28:4567–4582.

39. **EFSA Panel on Food Additives and Flavourings (FAF).** Re-evaluation of phosphoric acid–phosphates (E 338–341) as food additives. *EFSA Journal*. 2019;17(6):5674.

40. **Knappe DR, et al.** Adsorption of organic compounds from water. *Water Quality and Treatment*. 2011;16.1–16.107.

41. **Martinez ML, Torres MM, Guzman CA, Maestri DM.** Preparation and characteristics of activated carbon from olive stones and walnut shells. *Ind Crops Prod*. 2006;23(1):23–28.

42. **Jawad AH, Abd Rashid R, Ishak MAM, Wilson LD.** Adsorption of methylene blue onto activated carbon developed from biomass waste. *Desalin Water Treat*. 2016;57(52):25194–25206.

43. **Dadban Shahamat Y, Sadeghi M, Shahryari A, et al.** Heterogeneous catalytic ozonation of 2,4-dinitrophenol in aqueous solution. *Desalin Water Treat*. 2016;57(43):20447–20456.

44. **ASTM D3838-80.** Standard test method for pH of activated carbon. West Conshohocken: ASTM.

45. **Newcombe G, et al.** Adsorption of 2-methylisoborneol and geosmin on activated carbon: the importance of pore size distribution and surface chemistry. *Water Res*. 1997;31(8):2034–2046.

46. **Thommes M, et al.** Physisorption of gases, with special reference to the evaluation of surface area and pore size distribution (IUPAC Technical Report). *Pure Appl Chem*. 2015;87(9-10):1051–1069.

47. **ICH Guideline.** Validation of analytical procedures Q2 (R2). Geneva: ICH; 2023.

48. **El-Sayed GO, Yehia MM, Asaad AA.** Assessment of activated carbon prepared from corncob by chemical activation with phosphoric acid. *Water Res Indust*. 2014;7:66–75.

49. **Ibrahim M, Souleiman M, Salloum A.** Methylene blue dye adsorption onto activated carbon developed from *Calicotome villosa* via H3PO4. *Biomass Convers Biorefin*. 2023;13(14):12763–12776.

50. **Birbas D.** Preparation of activated carbon: forest residues activated with phosphoric acid and zinc sulfate [MSc thesis]. Stockholm: KTH; 2011.

51. **Wang B, Li Y, Si H, Chen H, Zhang M, Song T.** Analysis of the physical and chemical properties of activated carbons based on hulless barley straw and plain wheat straw obtained by H3PO4 activation. *BioResources*. 2018;13(3):5204–5212.

52. **Guo J, Lua AC.** Textural and chemical properties of adsorbent prepared from palm shell by phosphoric acid activation. *Mater Chem Phys*. 2003;80(1):114–119.

53. **Wiśniewska M, Urban T, Tokarska K, Marciniak P, Giel A, Nowicki P.** Removal of organic dyes, polymers and surfactants using carbonaceous materials derived from walnut shells. *Materials (Basel)*. 2024;17(9):1987.

54. **Davidi S, Lashanizadegan A, Sharififard H.** Walnut shell activated carbon: optimization of synthesis process, characterization and application for Zn(II) removal in batch and continuous process. *Mater Res Express*. 2019;6(8):085621.